

# Spontaneous and evoked activity in extended neural populations with gamma-distributed spatial interactions and transmission delay

Axel Hutt<sup>a,\*</sup>

<sup>a</sup>*Institute of Physics, Humboldt University of Berlin, Newtonstr. 15, 12489 Berlin, Germany*

Fatihcan M. Atay<sup>b</sup>

<sup>b</sup>*Max Planck Institute for Mathematics in the Sciences, Inselstr. 22, 04103 Leipzig, Germany.*

---

## Abstract

The spatiotemporal dynamics of neural activity are studied using an integro-differential model of spatially extended neuronal ensembles. The model includes both synaptic and axonal propagation delay while spatial synaptic connectivities are represented by gamma distributions. This family of connectivity kernels has been observed experimentally and covers the cases of divergent, finite, and negligible self-connections. We give conditions for stationary and nonstationary instabilities for gamma-distributed kernels, which can be formulated in terms of the mean spatial interaction ranges and the mean spatial interaction times. We present novel mechanisms for Turing patterns and traveling waves, which result from the special shape of the gamma-distributed interactions. We give a numerical study of the propagation of evoked spatiotemporal response activity caused by short local stimuli, and reveal maximum response activity after the mean interaction time. This maximum occurs at a distance from stimulus offset location, which is equal to the mean interaction range.

*Key words:* neuronal ensemble, synaptic connectivity kernel, bifurcation, stimulus response

*PACS:* 02.30.Rz, 87.18.Hf

---

\* Corresponding author

*Email addresses:* [Axel.Hutt@physik.hu-berlin.de](mailto:Axel.Hutt@physik.hu-berlin.de) (Axel Hutt),  
[atay@member.ams.org](mailto:atay@member.ams.org) (Fatihcan M. Atay).

*Preprint submitted to*

*To be published in Chaos, Solitons & Fractals*

## 1 Introduction

The dynamics of neuronal activity is responsible for such major brain functions as perception, memory processes or motor coordination. The present study aims to gain some insight into the rich neuronal behavior by studying spatiotemporal neuronal dynamics caused by fluctuations and environmental external stimuli.

Fluctuations in space and time are always present due to the large number of interconnected neurons and are supposed to be responsible for large-scale coherent phenomena near unstable neural activity states. We mention the phenomena of hallucinations, which frequently result from specific circumstances such as fatigue or sleep deprivation [1] and which, in some cases, exhibits a shift of the neural state to an instability by increased neuronal excitation [2,3]. For instance, Ermentrout and Cowan [4] introduced a mesoscopical neuronal field theory and explained visual hallucination patterns by loss of stability at bifurcation points.

In contrast, external stimuli may represent sensoric input as auditory speech or visual perceptions. For instance, during cognitive experiments encephalographic measurements reveal coherent evoked brain activity and indicate synchronous neuronal activity on a mesoscopic spatial level [5–9]. In this context, Freeman [10] has shown in an early study, that encephalographic activity relates to mesoscopic dendritic currents. Dipole and current source density models support these findings [11]. Hence, this study aims to study neuronal mechanisms on a spatially mesoscopic level.

Many studies investigating mesoscopic neuronal activity [12–20] treat synaptically coupled neuronal ensembles. This work follows the basic field approach of Jirsa and Haken [5], who combined the ensemble models of Wilson and Cowan [21] and Nunez [22]. This model considers a single type of neurons, which are interconnected by axons terminating at either excitatory or inhibitory synapses. Though the intrinsic delay due to axonal propagation had been introduced, it does not affect temporal and spatial dynamics. A recent work treating intracortical activity [23,24] extends the model by introducing synaptic response delay and thus adds a further time scale. It turns out, that the relation between synaptic and propagation delay affects the stability of the system.

In addition to the temporal scales, the synaptic connectivity kernels define the spatial scales of the neuronal field. In most studies, these connectivity kernels exhibit their maximum at zero distances, i.e. strong self-connectivity. Since experiments observed low probabilities [22] of local synaptic connections and the concerning effects of reduced self-connectivity has not been studied yet in

a general form, we shall discuss the family of gamma-distributed connectivity kernels. This special type of spatial interaction may exhibit infinite, finite, and negligible probability densities of self-connections for diverse parameters. These cases shall be studied in the context of spontaneous and externally evoked activity.

The paper is organized as follows. The subsequent section presents the derivation of the field equation. In Section 3, stability conditions with respect to spontaneous fluctuations are derived analytically, followed by a numerical study of evoked responses caused by external stimuli. Section 5 summarizes the results and closes the work.

## 2 The model

The present study treats a three-section model of synaptically coupled neuronal ensembles. Here, one section represents the ensemble set of synapses, which convert the incoming presynaptic activity to postsynaptic potentials (PSP). The adjacent model section contains the ensemble set of trigger zones at somata converting PSPs to axonal pulse activity while the final one represents the set of axonal fibres linking trigger zones to distant synapses. In the following, these model sections are discussed in some detail.

### 2.1 Model derivation

Chemical synapses convert incoming action potentials to postsynaptic currents by emission of neurotransmitters [25]. Most excitatory synapses (e) emit neurotransmitters called glutamate, which enhance the activity of the postsynaptic cells while the neurotransmitter  $\gamma$ -aminobutyric (GABA) emitted by inhibitory synapses (i) diminishes the postsynaptic cell activity. In addition, synapses may bind to dendrites or the soma of the postsynaptic neuron. Hence, the efficacy of synapses is very diverse. Furthermore, there is evidence, that the dendritic morphology, such as compactness of arborization and branching patterns, affects the stability of connected neurons [14], e.g. due to propagation delays along spatially extended dendrites. In a simplified model, dendrites are electric conductors which exhibit passive spread of current through the dendritic tissue. According to this approach, Freeman [26] was one of the first to show, that the response of chemical synapses to incoming action potentials is approximately equivalent to the convolution of the action potential with an impulse response function  $h_{e,i}(t)$ . The presented approach accounts for this finding and neglects shunting effects.

In experimental practice single cell activation is obtained frequently as the number of action potentials exceeding a certain threshold potential during a time interval. Hence it is reasonable to assume action potentials at discrete times and the mean pulse rate at time  $t$  gives the number of action potentials in the interval. This description yields a coarse-graining in time. In addition, the model introduces spatial patches at location  $x$  each containing a fixed number of synapses (typically  $\sim 10^4$ ). That means the activity discussed is coarse grained in space. Consequently, postsynaptic potentials averaged over time and space obey

$$\bar{V}^{e,i}(x, t) = \bar{g}_{e,i} \int_{-\infty}^t d\tau h_{e,i}(t - \tau) \bar{P}_{e,i}(x, \tau) , \quad (1)$$

with  $\bar{g}_{e,i}^{(l)}$  representing the efficacy of excitatory and inhibitory synapses while  $\bar{P}_{e,i}(x, t)$  are the presynaptic pulse rate coarse grained in time and space. The introduced spatial patches represent neuronal assemblies or neuronal pools [13,21,22,27], which build mesoscopic functional entities in the brain and have been found experimentally both in cortical [28,29] and subcortical [30] areas.

Now let us discuss the synaptic properties in more detail. According to [10], the impulse response function from (1) reads

$$h(t) = \frac{\alpha_1 \alpha_2}{\alpha_1 - \alpha_2} (e^{-\alpha_1 t} - e^{-\alpha_2 t}), \quad \alpha_1, \alpha_2 > 0 .$$

In case of  $\alpha_1 = \alpha_2 = \alpha$ , the function is the well-known alpha function  $h(t) = \alpha^2 t \exp(-\alpha t)$ . Moreover  $h(t)$  represents a Greens function for the temporal operator

$$\hat{L} = \left( \frac{\partial}{\partial t} + \alpha_1 \right) \left( \frac{\partial}{\partial t} + \alpha_2 \right)$$

with  $\hat{L}h(t) = \alpha_1 \alpha_2 \delta(t)$  and  $\delta(t)$  being the Dirac  $\delta$  function.

The adjacent model section focuses on the conversion of membrane potentials to pulse activity. A single neuron generates an action potential at time  $t$ , i.e. it fires if the membrane potential at the trigger zone exceeds a certain threshold. For an ensemble of neurons at spatial location  $x$ , there is a distribution of firing thresholds, as each neuron may exhibit different membrane conductivities. If these thresholds obey the time-independant normal distribution, the time-averaged pulse activity at location  $x$  maybe approximated by the logistic function [31,26,32–34]

$$\bar{N}(x, t) = P_{\max} S(V(x, t)) = \frac{P_{\max}}{1 + e^{-c(\hat{V}(x, t) - V_r)}} \quad (2)$$

with parameters  $c$ ,  $V_r$  defined in a later section.

To close the conversion chain of state variables, the final model section contains axonal fibres linking trigger zones and dendritic structures of terminal neurons. In mathematical terms, pulse activity generated at spatial location  $y$  propagates along axons by transmission speed  $v_{e,i}$  and sums up at the terminal excitatory and inhibitory synapses at the location  $x$  according to the corresponding axonal connectivity distributions  $f_e(x, y)$  and  $f_i(x, y)$ , respectively. More precisely, these distributions are the probability density of axonal connections between two spatial locations  $x$  and  $y$ . Thereby, the nonlocal interactions yield temporal propagation delays in case of finite axonal transmission speeds. Hence, the presynaptic pulse activity reads

$$\bar{P}_{e,i}(x, t) = \int_V dx' f_{e,i}(x, x') \hat{N}(x', t - \frac{|x - x'|}{v_{e,i}}) + \mu_{e,i} I(x, t) \quad (3)$$

with coupling factors  $\mu_{e,i}$ . The additional pulse activity  $I(x, t)$  introduces an external input, e.g. from other cortical regions or from the midbrain [22].

## 2.2 The field equation

Now, all model sections have been defined and we combine the major results (1), (2) and (3) to

$$\begin{aligned} \hat{L}V(x, t) = & \int_V a_e f_e(x, y) S(V(x', t - \frac{|x - y|}{v_e})) \\ & - a_i f_i(x, y) S(V(y, t - \frac{|x - y|}{v_i})) dy + \mu I(x, t) \end{aligned}$$

with  $a_{e,i} = \bar{g}_{e,i} P_{\max}$ ,  $\mu = \mu_e - \mu_i$ .

Many previous studies [4,23,35], neuronal fields exhibit axonal connections which are maximal at zero distance and monotonically decreasing for increasing distance. Then, the combination of excitatory and inhibitory axonal networks may yield four different spatial interactions, namely pure excitation, pure inhibition, local excitation-lateral inhibition and local inhibition-lateral excitation. In contrast, the current study takes into account the gamma distribution of cortico-cortical, i.e. excitatory, connections found in mice [22]. In addition, we set the corresponding inhibitory axonal distribution to a decreasing exponential [36]. Hence, it is

$$f_e(x, y) = \frac{1}{2r_e^p \Gamma(p)} |x - y|^{p-1} e^{-|x-y|/r_e}, \quad f_i(x, y) = \frac{1}{2r_i} e^{-|x-y|/r_i} \quad (4)$$

where  $p \in \mathfrak{R}$ ,  $p > 0$  is a parameter of the gamma distribution,  $\Gamma(p)$  denotes the gamma function and  $r_e, r_i$  are the spatial interaction range of excitatory and

inhibitory connectivity kernels, respectively. After scaling  $t \rightarrow t\sqrt{\alpha_1\alpha_2}$ ,  $x \rightarrow x/r_e$ ,  $v_{e,i} \rightarrow v_{e,i}/(r_e\sqrt{\alpha_1\alpha_2})$  the final field equation reads

$$\begin{aligned}\hat{L}V(x,t) &= \left( \frac{\partial^2}{\partial t^2} + \gamma \frac{\partial}{\partial t} + 1 \right) V(x,t) \\ &= \int_{-\infty}^{\infty} a_e K_e(x-y) S(V(y, t - \frac{|x-y|}{v_e})) \\ &\quad - a_i K_i(x-y) S(V(y, t - \frac{|x-y|}{v_i})) dy + \mu I(x,t)\end{aligned}\quad (5)$$

with

$$K_e(x) = \frac{1}{2\Gamma(p)} |x|^{p-1} e^{-|x|}, \quad K_i(x) = \frac{1}{2} r e^{-r|x|}, \quad (6)$$

$\gamma = (\alpha + \frac{1}{\alpha}) \geq 2$  and  $r = r_e/r_i$ . Equation (5) describes the dynamics of a coarse grained field of neuronal ensembles coupled by nonlinear, nonlocal interactions. It is damped by synaptic delay dynamics and subjected to delayed spatial interaction and external input. The mean spatial interaction ranges of excitatory and inhibitory connections, respectively, are given by

$$\xi_e = \int_{-\infty}^{\infty} dx K_e(x) |x| = p, \quad \xi_i = \int_{-\infty}^{\infty} dx K_i(x) |x| = 1/r$$

using Eq. (6).

In Figure 1, both kernels are plotted for various parameters  $p, r$  and we observe singular local excitations for  $p < 1$  (Fig. 1, left panel). At a first glance, this singularity of the probability density  $K_e$  may appear unphysical. However, this effect occurs even in much more simple processes and we mention the standard Brownian motion exhibiting a singular probability density of sojourn times [37,38].

### 3 Stability analysis

We consider the case of constant external input,  $\mu I(x,t) = I_0$ , and a stationary state  $V_0$  which is constant in space and time. Eq. (5) becomes the implicit equation

$$V_0 = (a_e - a_i) S(V_0) + I_0$$

which determines  $V_0$  subject to the external stimulus  $I_0$ . Now small deviations  $u(x,t) = V(x,t) - V_0$  around  $V_0$  obey

$$\hat{L}u(x,t) = s \int_{-\infty}^{\infty} a_e K_e(x-y) u(y, t - \frac{|x-y|}{v_e}) - a_i K_i(x-y) u(y, t - \frac{|x-y|}{v_i}) dy \quad (7)$$

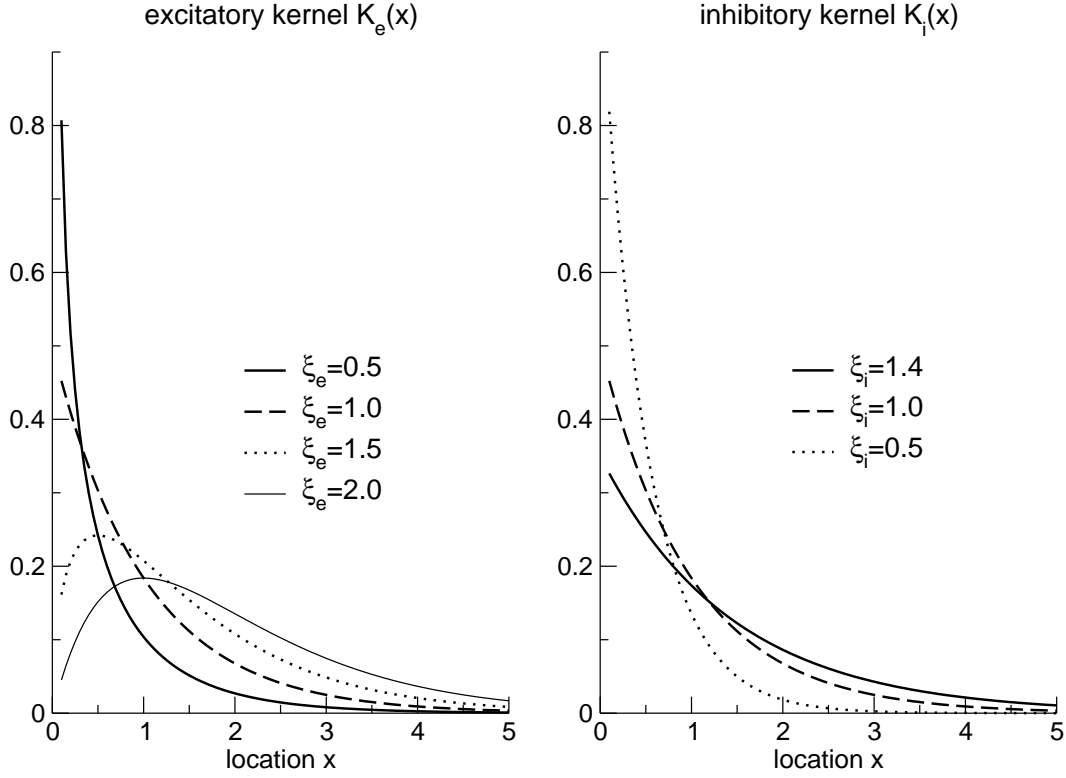


Fig. 1. Excitatory and inhibitory kernels for various parameters. All kernels are finite except for  $K_e(x)$  for  $p = 0.5$ . In case of  $p > 1$ , kernel  $K_e(x)$  exhibits a maximum far from the origin.

with the nonlinear gain  $s = \delta S / \delta V$  at  $V = V_0$ . With the ansatz  $u(x, t) = e^{\lambda t + ikx}$ , we obtain

$$L(\lambda) = s \int_{-\infty}^{\infty} dz \left( a_e K_e(z) e^{-\frac{\lambda}{v_e} |z|} - a_i K_i(z) e^{-\frac{\lambda}{v_i} |z|} \right) e^{ikz} \quad (8)$$

When  $s = 0$ , the above equation reduces to  $L(\lambda) = \lambda^2 + \gamma\lambda + 1 = 0$ , so that  $\text{Re } \lambda < 0$  and the perturbations  $u$  are damped out. It follows by continuity, that  $V_0$  is asymptotically stable for sufficiently small  $s$ . However, larger values of  $s$  may result in a loss of stability.

To study the stability of  $V_0$  in case of random fluctuations, we introduce small Gaussian fluctuations by letting  $\mu I(x, t) = I_0 + \Gamma(x, t)$ , with

$$\langle \Gamma(x, t) \rangle = 0, \quad \langle \Gamma(x, t) \Gamma(y, \tau) \rangle = Q' \delta(x - y) \delta(t - \tau),$$

where  $Q' < I_0^2$  is the fluctuation strength and  $\langle \cdot \rangle$  abbreviates the ensemble

average. Then Eq. (7) becomes

$$\begin{aligned} \hat{L}u(x, t) = & s \int_{-\infty}^{\infty} a_e K_e(x - y) u(y, t - \frac{|x - y|}{v_e}) \\ & - a_i K_i(x - y) u(y, t - \frac{|x - y|}{v_i}) dy + \Gamma(x, t), \end{aligned}$$

whose solution is [39]

$$\begin{aligned} u(x, t) = & u_h(x, t) \\ & + \frac{1}{\sqrt{2\pi}} \sum_{l=1}^m \int_0^t dt' \int_{-\infty}^{\infty} \tilde{\Gamma}(k, t') r_l(k) \exp [ikx + \lambda_l(k)(t - t')] dk. \end{aligned} \quad (9)$$

Here,  $u_h(x, t)$  represents the solution of Eq. (7),  $\tilde{\Gamma}(k, t)$  is the spatial Fourier transform of the Gaussian fluctuations with

$$\langle \tilde{\Gamma}(k, t) \rangle = 0, \quad \langle \tilde{\Gamma}(k, t) \tilde{\Gamma}(k', t') \rangle = Q \delta(k - k') \delta(t - t'),$$

$Q = Q'/\sqrt{2\pi}$ ,  $r_l(k) \in \Re$  are weight factors. Further,  $\lambda_l(k)$  are the roots of Eq. (8) of the finite number  $m$ . It is important to note, that in general Eq. (8) owns an infinite number of roots. However, the present study presumes large but finite transmission speeds, which yield the finite number of roots. Please see the section 3.3 for more details.

From Eq. (9) it turns out, that the stability of the field is given solely by  $\lambda_l(k)$  for finite random fluctuations  $\Gamma(k, t)$  [40]. These fluctuations represent small deviations from the stationary state and repel the system from its stationary state in case of  $Re(\lambda_l(k)) > 0$  and  $\Gamma(k, t) \neq 0$ . Since the sign of  $Re(\lambda)$  in Eq. (8) determines the stability at the presence of random fluctuations, the subsequent sections classify spontaneous instabilities by the values of  $\lambda$ .

### 3.1 Spontaneous stationary instability

At the stability threshold,  $Re(\lambda) = 0$ . In addition, for stationary bifurcations  $\lambda = 0$ , and the threshold for  $s$  is found from (8) as

$$s_c = \frac{1}{a_e \hat{K}_e(k_c) - a_i \hat{K}_i(k_c)} = \frac{1}{\hat{K}(k_c)},$$

where  $\hat{K}_e$  and  $\hat{K}_i$  are the Fourier transforms of  $K_e$  and  $K_i$ , respectively, and

$$\hat{K}(k) = \frac{a_e}{\sqrt{1 + k^{2p}}} \cos(p \arctan(k)) - a_i r^2 \frac{1}{r^2 + k^2}.$$

In case of a spatially constant bifurcation ( $k = 0$ ), the stationary state loses stability due to spontaneous fluctuations for

$$s > \frac{1}{\hat{K}(0)} = \frac{1}{a_e - a_i} .$$

On the other hand, for  $(a_e + a_i) > \hat{K}(k_c) > (a_e - a_i)$  a non-constant bifurcation may emerge with wavenumber  $k_c > 0$  and  $a_e > a_i$  [31]. The corresponding sufficient condition reads

$$\frac{\partial^2 \hat{K}(k)}{\partial k^2} \Big|_{k=0} > 0 \Rightarrow \xi_i^2 > \frac{a_e}{2a_i} \xi_e (\xi_e + 1)$$

with

$$\frac{\partial^2 \hat{K}(k)}{\partial k^2} = -\frac{a_e p(p+1)}{\sqrt{1+k^2}^{p+2}} \cos((p+2) \arctan(k)) + 2a_i r^2 \frac{r^2 - 3k^2}{(r^2 + k^2)^3},$$

which ensures a local maximum of  $\hat{K}(k)$  at finite  $k_c > 0$ . This bifurcation has been found first by Turing in non-equilibrium activator-inhibitor systems [41].

For  $\xi_e < 1$ , Turing patterns are present for  $\xi_i > \xi_e$  while for  $\xi_e \geq (a_e/a_i)/(2 - a_e/a_i)$ ,  $a_e \leq a_i$  they occur for  $\xi_i \leq \xi_e$  as well. This latter case reflects a larger mean excitation range than mean inhibition range and has not been found in previous studies. Moreover, Turing instabilities may also occur for  $\xi_e = 2$  although the kernel elicits local inhibition-lateral excitation interaction. Both latter novel cases are simulated in section 4.

### 3.2 Spontaneous non-stationary instability

A non-stationary bifurcation is characterized by a solution pair  $(\lambda, k)$  of (8) with  $\lambda = \pm i\omega$ ,  $\omega > 0$ . It can be shown, that such bifurcations are possible only if the transmission speeds  $v_{e,i}$  are not too large [31]. Indeed, considering the imaginary part of (8) gives

$$\omega\gamma = -2s \int_0^\infty dz (a_e K_e(z) \sin(\omega z/v_e) - a_i K_i(z) \sin(\omega z/v_i)) \cos(kz)$$

using the fact, that integrands which are odd functions over  $(-\infty, \infty)$  have vanishing integrals. Employing the estimate  $|\sin x| \leq |x|$  one obtains

$$|\omega|\gamma \leq 2s \int_0^\infty dz (a_e |K_e(z)\omega z/v_e| + a_i |K_i(z)\omega z/v_i|)$$

and since  $\omega \neq 0$  at a non-stationary bifurcation,

$$\gamma \leq s \left( \frac{a_e}{v_e} \int_0^\infty dz 2K_e(z)z + \frac{a_i}{v_i} \int_0^\infty dz 2K_i(z)z \right).$$

The integrals express the mean spatial interaction ranges  $\xi_e$  and  $\xi_i$  for excitatory and inhibitory connections, respectively. Hence we define

$$\tau_e = \frac{1}{v_e} \int_{-\infty}^\infty dz K_e(z)|z| = \xi_e/v_e, \quad \tau_i = \frac{1}{v_i} \int_{-\infty}^\infty dz K_i(z)|z| = \xi_i/v_i$$

as the mean delay times respectively for the excitatory and inhibitory information transmission in the field. Thus, a necessary condition for non-stationary bifurcations to occur is

$$s \geq s_c = \frac{\gamma}{a_e\tau_e + a_i\tau_i}. \quad (10)$$

For the particular case when the distributions are given by (6), we have

$$\frac{\gamma}{s} \leq \frac{a_e p}{v_e} + \frac{a_i/r}{v_i}$$

by using the mean values of the gamma and exponential probability density distributions. This relation elicits a decreased threshold  $s_c$  for increased values of  $p$  and  $1/r$ , i.e. the larger  $p$  and  $1/r$  the easier nonstationary bifurcations may occur.

With Eq. (10) and the previous condition  $1/(a_e + a_i) < s < 1/(a_e - a_i)$  for nonconstant bifurcations, the parameter regime for nonstationary bifurcation is given by

$$\frac{\gamma}{\tau_e \frac{a_e}{a_i} + \tau_i} < a_i s < \frac{1}{\frac{a_e}{a_i} - 1}, \quad \frac{1}{\frac{a_e}{a_i} + 1} < a_i s$$

As can be shown by simple calculus, there is a threshold

$$a_e/a_i = \frac{\gamma + \tau_i}{\gamma - \tau_e}, \quad \tau_e < \gamma$$

beyond which no nonstationary bifurcations occur while  $\tau_e > \gamma$  allows nonstationary bifurcations for all  $a_e/a_i \geq 1$ . The novel oscillatory space-time activity for local-excitation lateral-inhibition interactions is discussed numerically in the subsequent section.

### 3.3 Evoked stimulus response

Now, we aim to examine the evoked response of the system to external stimuli. For simplicity, in this section it is  $v_e = v_i = v$  and  $K(x) = a_e K_e(x) - a_i K_i(x)$ .

Thus Eq. (7) reads

$$\hat{L}_t u(x, t) = s \int_{-\infty}^{\infty} dy K(x-y) u(y, t - \frac{|x-y|}{v}) + E(x, t).$$

with the external stimulus  $E(x, t)$ . With the Greens function  $G(x, t)$ , it is

$$u(x, t) = \frac{1}{2\pi} \int_{-\infty}^{\infty} dx' \int_{-\infty}^{\infty} dt' G(x-x', t-t') E(x', t')$$

and the application of the Fourier transform yields

$$\left[ L(-i\omega) e^{ik(x-x')} - s \int_{-\infty}^{\infty} dy \underbrace{K(x-y) e^{i\omega|x-y|/v}}_{F(x-y, \omega)} e^{ik(y-x')} \right] \tilde{G}(k, \omega) = \frac{1}{2\pi} e^{ik(x-x')}.$$

Here,  $\tilde{G}(k, \omega)$  represents the Fourier transform in space and time of the Greens function. Some more calculations lead to

$$\tilde{G}(k, \omega) = \frac{1}{2\pi} \frac{1}{L(-i\omega) - s\sqrt{2\pi}\tilde{F}(k, \omega)},$$

where  $\tilde{F}(k, \omega)$  is the Fourier transform of  $F(x, \omega)$ . For large transmission speeds  $v$  it is

$$\begin{aligned} \tilde{F} &= \frac{1}{\sqrt{2\pi}} \int_{-\infty}^{\infty} dz K(z) e^{i\omega|z|/v} e^{ikz} \approx \sum_{l=0}^N \frac{1}{l!} \left(\frac{i\omega}{v}\right)^l \int_{-\infty}^{\infty} dz |z|^l K(z) e^{ikz} \\ &\approx \frac{1}{\sqrt{2\pi}} \sum_{l=0}^N \frac{1}{l!} \tilde{K}_l(k). \end{aligned}$$

In the following  $\tilde{K}_l(k)$  is called the kernel Fourier moments of  $l$ -th order. Then for finite number of kernel Fourier moments  $N$  the Fourier transform of the Greens function in  $k$ -space reads

$$g(k, t) = \frac{1}{\sqrt{2\pi}^3} \int_{-\infty}^{\infty} d\omega \frac{e^{-i\omega t}}{L(-i\omega) - s\sqrt{2\pi}\tilde{F}(k, \omega)} \quad (11)$$

$$= \mathcal{R} \left\{ \frac{1}{\sqrt{2\pi}^3} \int_{\mathcal{C}} d\Omega \frac{e^{-i\Omega t}}{L(-i\Omega) - s\sqrt{2\pi}\tilde{F}(k, \Omega)} \right\} = \mathcal{R} \left\{ \frac{i}{\sqrt{2\pi}} \sum_{m=1}^M Res(\Omega_m) \right\} \quad (12)$$

Here,  $\mathcal{R}$  denotes the real part. According to the residue theory,  $Res(\Omega_m)$  represents the residuum of the integrator in (11) at the  $M$  singularities  $\Omega_m$  while the complex integral in (12) is closed along the path  $\mathcal{C}$ . The choice of  $\mathcal{C}$  depends strongly on the singularities  $\Omega_m$ , i.e. the roots of  $L(-i\Omega_k) - s\sqrt{2\pi}\tilde{F}(k, \Omega_k) = 0$ . For finite  $N$ , the number of these roots  $M$  is finite and the

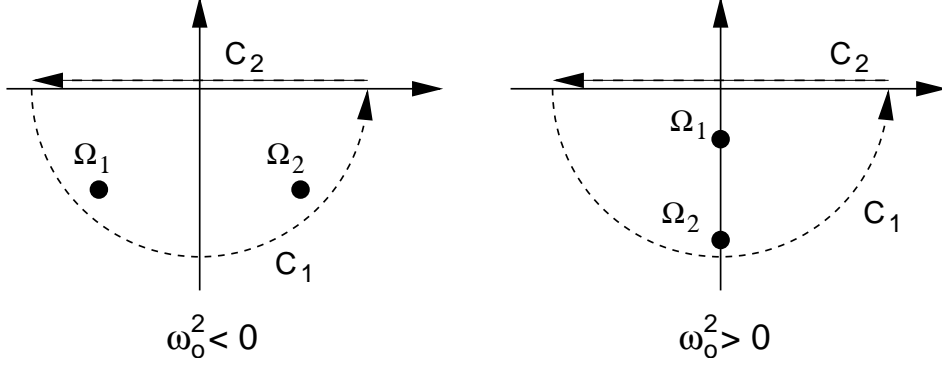


Fig. 2. The integration paths in the complex plane.

path  $\mathcal{C}$  encloses a finite regime in the complex plane. Subsequently Eq. (12) is valid.

Considering terms up to second order, i.e. short-range interactions with  $N = 2$ , the roots are given by

$$\Omega_{1,2} = \frac{1}{2A(k)} \left( iB(k) \pm \sqrt{\omega_0^2} \right) \quad (13)$$

with

$$\omega_0^2 = -B^2(k) - 4A(k)C(k), \quad A(k) = -1 + s\tilde{K}_2(k)/(2v^2) \quad (14)$$

$$B(k) = \gamma s\tilde{K}_1(k)/v, \quad C(k) = 1 - s\tilde{K}_0(k)$$

and  $\tilde{K}_0 = \tilde{K}$ . Figure 2 shows the complex plane with the two different cases  $\omega_0^2 > 0$  and  $\omega_0^2 < 0$  with  $A < 0$ ,  $B > 0$  and  $C > 0$ , i.e.  $s/v^2 < 2/\tilde{K}_2(k)$ ,  $s/v < -\gamma/\tilde{K}_1(k)$  and  $s < 1/\tilde{K}(k)$  for all  $k$ . According to previous studies [24], the latter two conditions prohibits stationary and non-stationary bifurcations and thus guarantee asymptotic stability of  $V_0$ .

The closed path  $\mathcal{C} = \mathcal{C}_1 + \mathcal{C}_2$  separates into the half circle  $\mathcal{C}_1$  and the path  $\mathcal{C}_2$  along the real axis. With  $\Omega = R \exp(i\phi)$ ,  $-\pi < \phi < 2\pi$ , we find

$$\int_{\mathcal{C}_1} \frac{e^{-i\Omega t}}{L(-i\Omega) - s\sqrt{2\pi}\tilde{F}(k, \Omega)} d\Omega \rightarrow 0 \quad \forall R \rightarrow \infty, \quad t \geq 0.$$

Here, the positive sign of  $t$  guarantees causality. Further some calculations yield for  $\omega_0^2 > 0$

$$g(k, t) = \frac{2}{\sqrt{2\pi}\omega_0(k)} e^{-B(k)t/2|A(k)|} \sin \frac{\omega_0(k)}{2|A(k)|} t$$

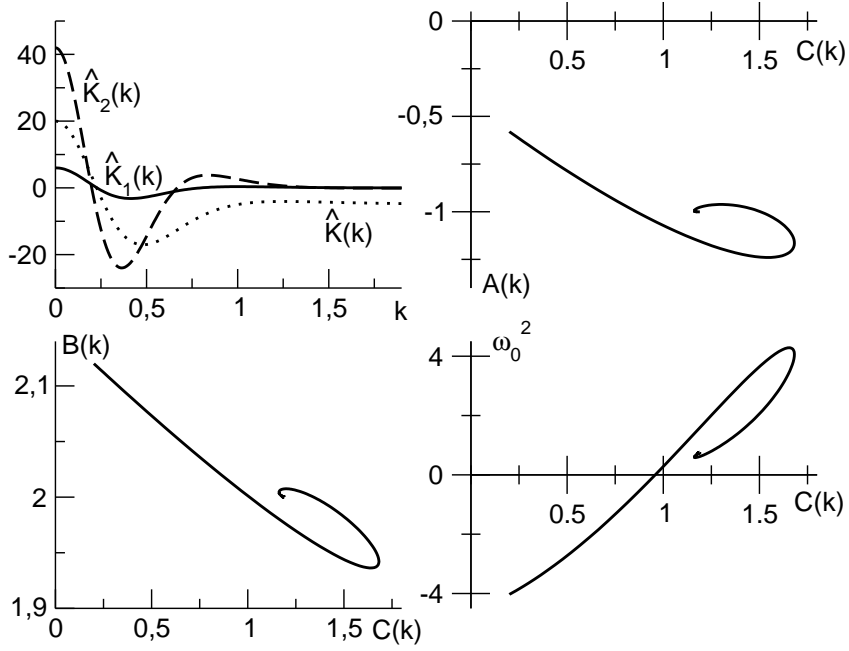


Fig. 3. Variables of Eq. (13) subject to  $k$ . Top row, left panel: the first three kernel Fourier moments for a typical local inhibition-lateral excitation kernel  $K(x)$ ; top row, right panel and bottom row, left panel: plot of the three variables  $A(k)$ ,  $B(k)$  and  $C(k)$ , which depend on the kernel Fourier moments by Eq.(14); bottom row, right panel: values of  $\omega_0^2$  subject to  $k$ .

and for  $\omega_0^2 < 0$

$$g(k, t) = \frac{2}{\sqrt{2\pi}\sqrt{-\omega_0^2(k)}} e^{-B(k)t/2|A(k)|} \sinh \frac{\sqrt{-\omega_0^2(k)}}{2|A(k)|} t.$$

We point out, that values of  $k$  determine the sign of  $\omega_0^2$ . Figure 3 shows plots of the kernel Fourier modes and  $A$ ,  $B$ ,  $C$  and  $\omega_0^2$  with respect to  $k$ . Hence, the field evolution is given by

$$u(x, t) = \frac{1}{2\pi} \int_{-\infty}^t dt' \int_{-\infty}^{\infty} dy \int_{-\infty}^{\infty} dk g(k, t - t') e^{ik(x-y)} E(y, t')$$

while  $g(k, t)$  is chosen in correspondence to the sign of  $\omega_0^2(k)$ .

In order to illustrate the findings, let us expand the stimulus  $E(x, t)$  by spatial Fourier series and assume a block stimulus, which sets in at  $t = 0$  with duration  $\Delta T$ , i.e.

$$E(x, t) = \sum_{n=1}^{\infty} (M_n \cos(k_n x) + N_n \sin(k_n x)) (\Theta(t) - \Theta(t - \Delta T)).$$

Then we obtain for  $t \geq \Delta T$

$$u(x, t) = \sum_{n=1}^{\infty} D_n(x) \int_0^{\Delta T} dt' \frac{e^{-B(k_n)(t-t')/2|A(k_n)|}}{\omega_0(k_n)} \sin\left(\frac{\omega_0(k_n)}{2|A(k_n)|}(t-t')\right) \quad (15)$$

for  $\omega_0^2(k_n) > 0$ ,

$$u(x, t) = \sum_{n=1}^{\infty} D_n(x) \int_0^{\Delta T} dt' \frac{e^{-B(k_n)(t-t')/2|A(k_n)|}}{\sqrt{-\omega_0^2(k_n)}} \sinh\left(\frac{\sqrt{-\omega_0^2(k_n)}}{2|A(k_n)|}(t-t')\right) \quad (16)$$

for  $\omega_0^2(k_n) < 0$  and  $\omega_0^2(k_c) = 0$  leads to

$$u(x, t) = D_c(x) \int_0^{\Delta T} dt' \frac{e^{-B(k_c)(t-t')/2|A(k_c)|}}{2|A(k_c)|} (t-t'). \quad (17)$$

with  $D_n(x) = 2M_n \cos(k_n x) + 2N_n \sin(k_n x)$ . The integrals in Eqs. (15), (16), (17) determine the temporal behaviour of the response and their evolution in time is shown in Fig. 4 for various  $k$ . We observe a temporal response maximum at

$$\tan(\beta t_0) = \sin(\beta \Delta T) / (\cos(\beta \Delta T) - \exp(-\alpha \Delta T))$$

for  $\omega_0^2 > 0$  and

$$\tanh(\beta t_0) = \sinh(\beta \Delta T) / (\cosh(\beta \Delta T) - \exp(-\alpha \Delta T))$$

for  $\omega_0^2 < 0$  with  $\beta = \omega_0/2|A|$  and  $\alpha = -B/2|A|$ . In case of vanishing propagation delay,  $|A| = 1$  and  $B = \gamma$  are constant while  $C = C(k)$ , i.e. the response maximum still depends on  $k$  in case of vanishing propagation delay.

#### 4 Numerical analysis

Now we aim to simulate the spontaneous and the evoked neural activity. For the numerical investigations the parameters of the sigmoidal function  $S(V)$  is chosen physiologically reasonable as  $c = 1.8$ ,  $V_r = 3.0$  [42]. The subsequent temporal integration procedure applies an explicit Euler algorithm while the spatial integration algorithm obeys

$$\int_0^L f(z) dz \approx \sum_{i=1}^N \frac{1}{2} (f(z_i) + f(z_{i+1})) dx \quad (18)$$

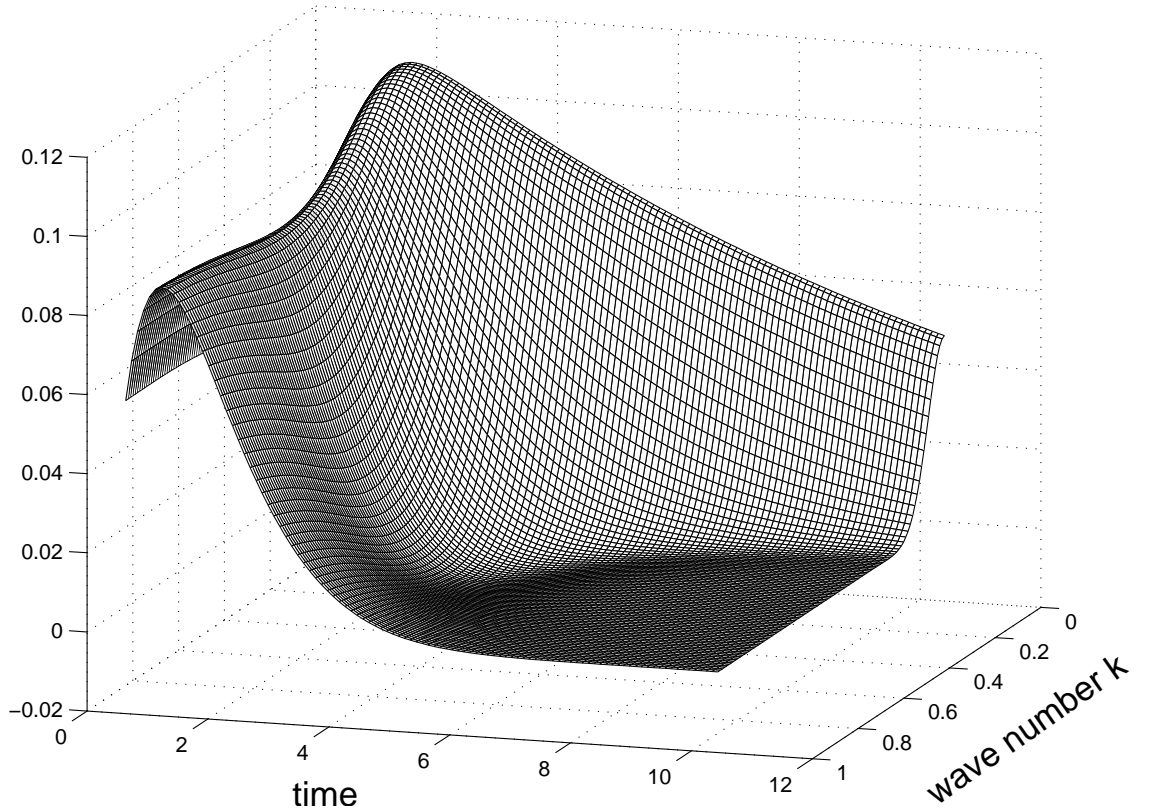


Fig. 4. Plot of the integral of Eqs. (15),(16) and (17) showing the temporal evolution of the system.

for an integrand  $f$  and the field length  $L$  with  $N = L/dx$ . Furthermore, periodic boundary conditions are set, yielding

$$\int_{-\infty}^{\infty} K(|x-y|)f(y)dy \approx \int_0^L K(L/2 - |L/2 - |x-y||)f(y)dy.$$

Initial values  $V^0(x,t) = V_0$  for  $-L/v_e \leq t \leq 0$  guarantee negligible initial transients.

#### 4.1 Spontaneous activity

For the simulation of spontaneous activity, the spatial field exhibits  $N = 200$  discrete elements with width  $dx = 0.3$ , the temporal iteration is applied with the time interval  $dt = 0.06$  and the transmission speeds are set  $v_e = v_i = v$ . This equivalence of both transmission speeds is a reasonable assumption for intracortical fields [23]. Further parameters are given in the corresponding figures. Fig. 5 shows the novel Turing instability for local inhibition and lateral excitation while Fig. 6 presents the novel wave instability for local excitation

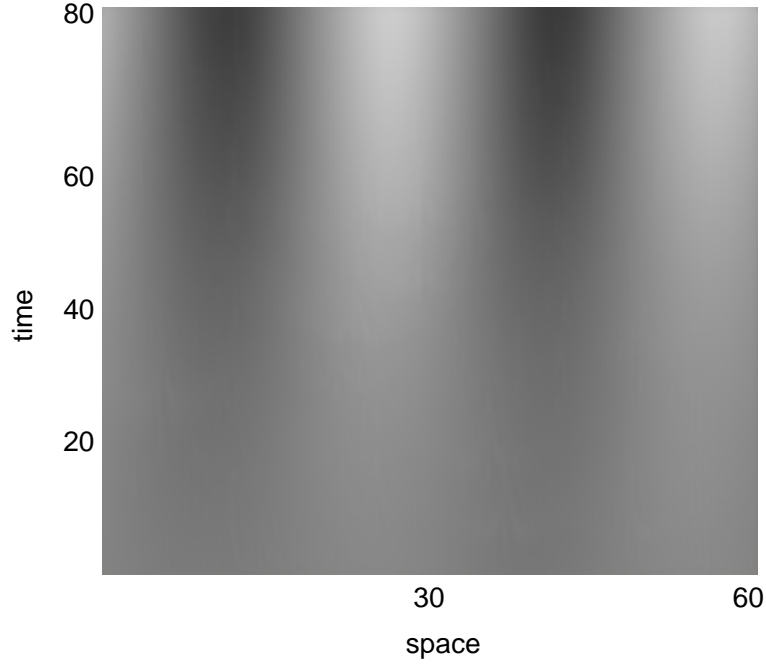


Fig. 5. Space-time plot revealing the Turing instability for local inhibition-lateral excitation interaction. Parameters are set to  $\xi_e = 2.0$ ,  $\xi_i = 1.92$ ,  $a_e = 131.0$ ,  $a_i = 130.0$ ,  $v_e = v_i = 10.0$ ,  $\gamma = 2.0$ . The greyscale encodes the deviation from the stationary state.

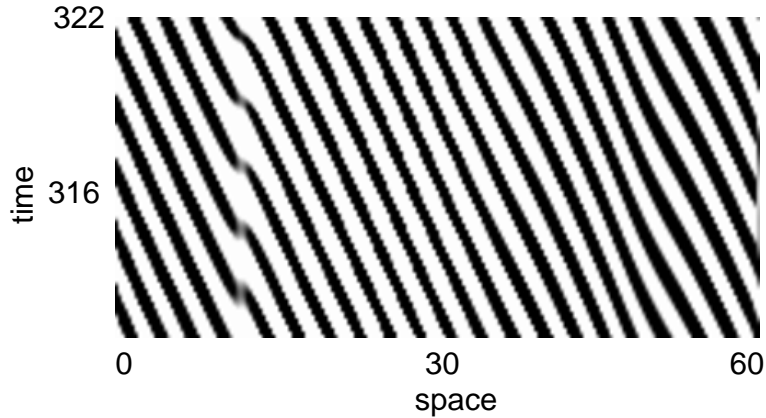


Fig. 6. Space-time plot revealing the wave instability for local excitation-lateral inhibition interaction. Parameters are set to  $\xi_e = 0.9$ ,  $\xi_i = 0.5$ ,  $a_e = 10.0$ ,  $a_i = 7.5$ ,  $v_e = v_i = 1.66$ ,  $\gamma = 0.2$ . The greyscale encodes the deviation from the stationary state.

and lateral inhibition.

#### 4.2 Evoked stimulus response

Essentially we aim to extract further spatiotemporal properties from the neural system for different excitatory spatial ranges  $\xi_e$ . In experimental practice,

neural tissue is stimulated by local external input during a finite time interval. We choose the external stimulus to be

$$I(x, t) = I_0 + \begin{cases} I_{local} & : \quad x_0 \leq x \leq x_0 + \Delta x, \quad 0 \leq t \leq \Delta T \\ 0 & : \quad \text{otherwise} \end{cases}$$

For the numerical investigations additional parameters are chosen to  $\alpha_1 = \alpha_2 = 200\text{Hz}$  [43,44], i.e.  $\gamma = 2$ . Further, spatial ranges are  $r_e = 20\text{mm}$ ,  $r_i \approx 1\text{mm}$  [22], i.e.  $\xi_i = 0.05$ , and  $\xi_e = 3$ . The spatial field exhibits  $N = 400$  discrete elements each of the length  $dx = 1\text{mm}$  while the time period is discretized by 100 time steps each of duration  $dt = 0.4\text{ms}$ . In addition, the transmission speed along excitatory axonal connections is  $v_e = 8\text{m/s}$  while the delay along short-range inhibitory connections is neglected. For synaptic parameters  $a_e = 25$ ,  $a_i = 5$  the constant external stimulus  $I_0 = 0.1$  guarantees asymptotic stability at the stationary state  $V_0 = 0.23$ . Then the additional local stimulus of strength  $I_{local} = 5$  of width  $\Delta x = 10\text{mm}$  and duration  $\Delta T = 8\text{ms}$  evokes spatiotemporal activity, which is shown as space-time plots in Fig. 7 for various excitatory spatial ranges  $\xi_e = p$ . During stimulation no activity spreads into the field. In contrast after stimulus offset activation travels from the stimulus center. Graphical evaluations reveal, that the activation propagates with the transmission speed  $v_e$  and exhibits its maximum at a distance  $\xi_e \cdot r_e$  from stimulus offset location, i.e. at the mean excitatory interaction range. Hence, the expected time for maximum stimulus response is the mean interaction time  $\tau_e$ . This result coincides for all parameters  $\xi_e = p$  in Fig. 7.

Finally, we examine the activity response evoked by a different stimulus

$$I(x, t) = I_0 + \begin{cases} 5.0 \cdot \cos(k_0 x) & : \quad 0 \leq t \leq \Delta T \\ 0 & : \quad \text{otherwise} \end{cases}$$

for the same parameters as above. Figure 8 shows results for two different values of  $k_0$ . We observe diverse periodic spatiotemporal patterns, which reveal the spatial periodicity of the stimulus and again exhibit the mean excitatory interaction time as the occurrence time of global maximum activity.

## 5 Conclusion

The present work discusses a model for nonlocally interacting neural populations. It considers synaptic and axonal propagation delay effects besides general gamma-distributed excitatory and inhibitory axonal connectivities.

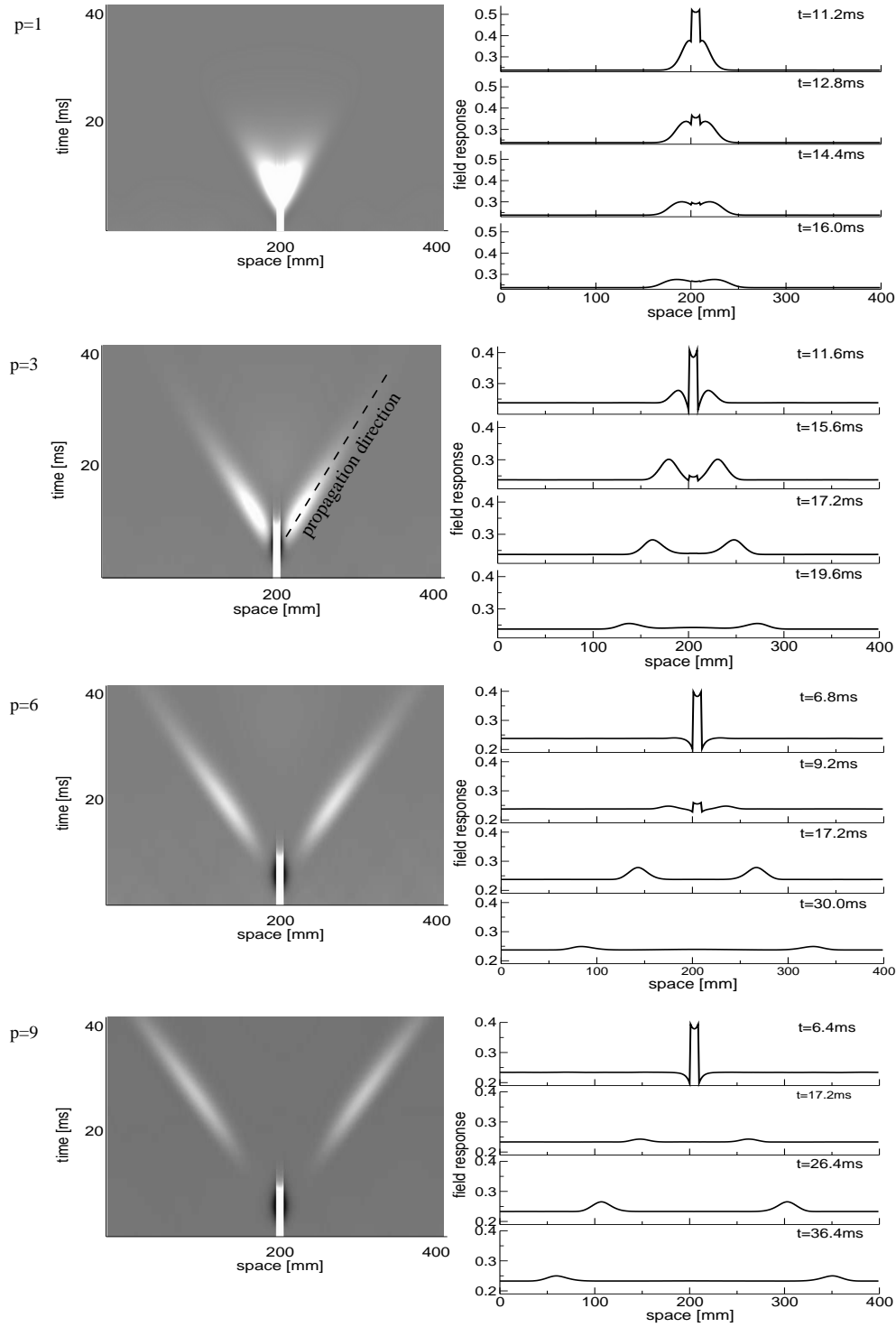


Fig. 7. Spatiotemporal stimulus response to a local stimulation for various parameters  $\xi_e = p$ . Left column: Space-time plots of field activity while the greyscale encodes positive (white) and negative (black) deviations from the stationary state (grey). The activity  $V$  has been clipped for  $|V - V_0| > 0.05$  due to illustrative reasons, i.e. equal-greyscaled areas occur due to clipping. Activity transmission speeds are computed for all  $p$  along estimated lines which are similar to the dashed line plotted for  $p = 3$ . Right column: several time samples of spatial activity for the corresponding values of  $p$ .

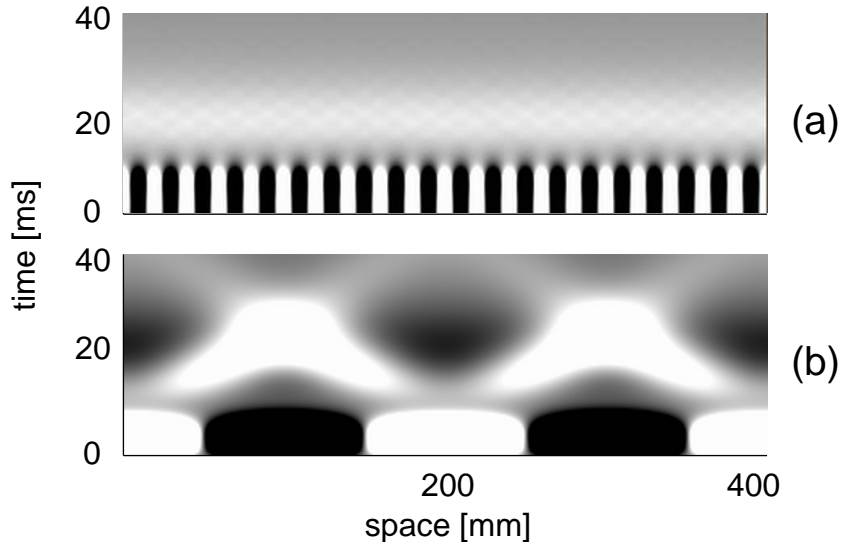


Fig. 8. Spatiotemporal stimulus response to a spatially periodic stimulus. The parameters are (a)  $k_0 = 2\pi/20 \text{ mm}^{-1}$  and (b)  $k_0 = 2\pi/200 \text{ mm}^{-1}$ . The greyscale encoding is the same as in Fig. 7.

The neural population is studied with respect to its stability towards random fluctuations and external stimuli. We find two novel mechanisms for pattern formation, namely Turing patterns for local inhibition-lateral excitation and travelling waves for local excitation-lateral inhibition. Moreover conditions for stationary and nonstationary instabilities exhibit only a few parameters. That is, mean excitatory and inhibitory spatial interaction ranges define the sufficient parameter regime of spontaneous Turing patterns while mean excitatory and inhibitory interaction times determine the necessary parameter regime of spontaneous nonstationary phenomena. Interestingly, these parameters also appear to play an important role in the evoked response activity caused by local external stimuli. In the numerical study, evoked activation propagates at axonal transmission speed and its maximum occurs at a distance from stimulus onset equal to the mean spatial interaction range after the corresponding mean interaction time. This rather intuitive finding gives new insights to stimulus responses in nonlocally interacting fields and, especially, to information processing in local brain areas during cognitive processing of external stimuli. Future work shall discuss evoked responses analytically subjected to diverse stationary and nonstationary spatiotemporal stimuli.

## References

- [1] J. R. Brasic, Hallucinations, *Percep. Motor Skills* 86 (1998) 851–877.
- [2] S. H. Isaacson, J. Carr, A. J. Rowan, Ciprofloxacin-induced complex partial status epilepticus manifesting as an acute confusional state, *Neurol.* 43 (1993) 1619
- [3] P. Tass, Oscillatory cortical activity during visual hallucinations, *J. Biol. Phys.* 23 (1997) 21–66.
- [4] G. B. Ermentrout, J. D. Cowan, A mathematical theory of visual hallucination patterns, *Biol. Cybern.* 34 (1979) 137
- [5] V. K. Jirsa, H. Haken, Field theory of electromagnetic brain activity, *Physical Review Letters* 7 (5) (1996) 960–963.
- [6] C. Uhl (Ed.), *Analysis of Neurophysiological Brain Functioning*, Springer-Verlag, Berlin, 1999.
- [7] A. Hutt, H. Riedel, Analysis and modeling of quasi-stationary multivariate time series and their application to middle latency auditory evoked potentials, *Physica D* 177 (2003) 203
- [8] H. Haken, *Principles of Brain Functioning*, Springer, Berlin, 1996.
- [9] W. J. Freeman, *Neurodynamics: An Exploration in Mesoscopic Brain Dynamics (Perspectives in Neural Computing)*, Springer-Verlag, Berlin, 2000.
- [10] W. J. Freeman, A model for mutual excitation in a neuron population in olfactory bulb, *IEEE Trans. Biomed. Engin.* 21 (1974) 350
- [11] J. C. Mosher, P. S. Lewis, R. M. Leahy, Multiple dipole modeling and localization from spatio-temporal meg-data, *IEEE Trans. Biomed. Eng.* 39 (6) (1992) 541
- [12] P. A. Robinson, P. N. Loxley, S. C. O’Connor, C. J. Rennie, Modal analysis of corticothalamic dynamics, electroencephalographic spectra and evoked potentials, *Physical Review E* 63 (2001) 041909.
- [13] W. Gerstner, Time structure of the activity in neural network models, *Phys. Rev. E* 51 (1) (1995) 738–758.
- [14] P. C. Bressloff, S. Coombes, Physics of the extended neuron, *Int. J. Mod. Phys. B* 11 (20) (1997) 2343–2392.
- [15] B. Ermentrout, Neural networks as spatio-temporal pattern-forming systems, *Reports on Progress in Physics* 61 (1998) 353–430.
- [16] W. M. Kistler, R. Seitz, J. L. van Hemmen, Modeling collective excitations in cortical tissue, *Physica D* 114 (1998) 273–295.
- [17] R. Ben-Yishai, R. L. Bar-Or, H. Sompolinsky, Theory of orientation tuning in visual cortex, *Proc. Natl. Acad. Sci.* 92 (1995) 3844

- [18] T. Wennekers, Dynamic approximation of spatio-temporal receptive fields in nonlinear neural field models, *Neural Computation* 14 (2002) 1801–1825.
- [19] J. Eggert, J. L. van Hemmen, Unifying framework for neuronal dynamics, *Phys. Rev. E* 61 (2) (2000) 1855
- [20] T. D. Frank, A. Daffertshofer, P. J. Beek, H. Haken, Impacts of noise on a field theoretical model of the human brain, *Physica D* 127 (1999) 233–249.
- [21] H. R. Wilson, J. D. Cowan, Excitatory and inhibitory interactions in localized populations of model neurons, *Biophys. J.* 12 (1972) 1–24.
- [22] P. L. Nunez, *Neocortical dynamics and human EEG rhythms*, Oxford University Press, New York - Oxford, 1995.
- [23] A. Hutt, M. Bestehorn, T. Wennekers, Pattern formation in intracortical neuronal fields, *Network: Comput. Neural Syst.* 14 (2003) 351–368.
- [24] F. M. Atay, A. Hutt, Stability and bifurcations in neural fields with finite propagation speed and general connectivity, *SIAM J. Appl. Math.* 65 (2) (2005) 644–666.
- [25] J. C. Eccles, M. Ito, J. Szentagothai, *The Cerebellum as a Neuronal Machine*, Springer-Verlag, New York, 1967.
- [26] W. J. Freeman, *Mass Action in the Nervous System*, Academic Press, New York, 1975.
- [27] J. Eggert, J. L. van Hemmen, Modeling neuronal assemblies: Theory and implementation, *Neural Comput.* 13 (9) (2001) 1923
- [28] V. B. Mountcastle, Modality and topographic properties of single neurons of cat’s somatic sensory cortex., *Neurophysiol.* 20 (1957) 408
- [29] D. H. Hubel, T. N. Wiesel, Receptive fields of cells in striate cortex of very young, visually unexperienced kittens, *J. Physiol* 26 (1963) 994
- [30] K. J. Sanderson, The projection of the visual field to the lateral geniculate and medial interlaminar nuclei in the cat, *J. Comp. Neurol.* 143 (1971) 101
- [31] A. Hutt, F. M. Atay, Analysis of nonlocal neural fields for both general and gamma-distributed connectivities, *Physica D* 203 (2005) 30–54.
- [32] W. J. Freeman, Nonlinear gain mediating cortical stimulus-response relations, *Biological Cybernetics* 33 (1979) 237–247.
- [33] W. A. Little, The existence of persistent states in the brain, *Math. Biosc.* 19 (1974) 101
- [34] J. J. Wright, D. T. J. Liley, Simulation of electrocortical waves, *Biological Cybernetics* 72 (1995) 347–356.
- [35] H. R. Wilson, J. D. Cowan, A mathematical theory of the functional dynamics of cortical and thalamic nervous tissue, *Kybernetik* 13 (1973) 55–80.

- [36] G. Tamas, E. H. Buhl, P. Somogyi, Massive autaptic self-innervation of gabaergic neurons in cat visual cortex, *J. Neurosci.* 17 (16) (1997) 6352
- [37] P. Levy, Sur certains processus stochastique homogènes, *Comp. Math.* 7 (1939) 283
- [38] W. Feller, *An introduction to probability theory and its applications*, Wiley, New York, 1966.
- [39] A. Hutt, T. D. Frank, Critical fluctuations in neural fields, in preparation (2005).
- [40] A. A. Gushchin, U. Kuechler, On stationary solutions of delay differential equations driven by a lévy process, *Stochastic Proc. Appl.* 88 (2000) 195–211.
- [41] A. M. Turing, The chemical basis of morphogenesis, *Philos. Trans. R. Soc. London* 327B (1952) 37–72.
- [42] J. J. Wright, D. T. J. Liley, A millimetric-scale simulation of electrocortical wave dynamics based on anatomical estimates of cortical synaptic density, *Biosystems* 63 (2001) 15–20.
- [43] F. H. L. da Silva, A. Hoeks, A. Smits, L. H. Zetterberg, Model of brain rhythmic activity, *Kybernetik* 15 (1974) 24
- [44] P. A. Robinson, C. J. Rennie, J. J. Wright, Propagation and stability of waves of electrical activity in the cerebral cortex, *Physical Review E* 56 (1) (1997) 826–840.